2D(r,θ) simulations of the HBC-4 power-to-melt experiment with the fuel performance code ALCYONE

J. Sercombe, V. D'ambrosi, S. Béjaoui, I. Zacharie-Aubrun

2D(r,θ) simulations of the HBC-4 power-to-melt experiment with the fuel performance code ALCYONE

J. Sercombe[a,*], V. D'Ambrosi[a], S. Béjaoui[a], I. Zacharie-Aubrun[a]

[a] *CEA,DES, IRESNE,DEC, F- 13108 St-Paul-lez-Durance - France.*

Abstract

This paper presents 2D(r,θ) simulations of the HBC-4 power-to-melt experiment performed with the fuel performance code ALCYONE. The HBC-4 experiment is one of the two test cases selected for the Simulation exercise on past fuel melting experiments of the Power to Melt and Maneuverability (P2M) project. The Ramp Terminal Level (RTL) at Peak Power Node (PPN) has been estimated at 66 kW.m^{-1} by gamma scanning and 70 kW.m^{-1} based on online measurements of thermal fluxes. The fuel burnup at PPN was close to 60 GWd.tU^{-1}. The cladding failed during the short holding time at RTL of 40 s. Fuel melting took place at the pellet center and in particular in front of clad cracks.

In this paper, simulations of the HBC-4 power-to-melt experiment are performed using an updated version of the 2D(r,θ) scheme of ALCYONE where half of the fuel pellet is described. This configuration allows the modeling of clad failure by Iodine Stress Corrosion Cracking, and of its consequences on the fuel pellet deformation. The modeling of fuel melting relies on thermochemical equilibrium calculations performed with the OpenCalphad Gibbs Energy Minimizer and the Thermodynamics of Advanced Fuels International Database (TAF-ID).

The simulation without clad failure indicates that the solidus is reached during the HBC-4 experiment but not the liquidus. The simulation with clad failure leads to a small increase of the fuel temperature that is sufficient to reach the liquidus at the pellet center, in agreement with Post Irradiation Examination (PIE). The impact of water ingress in the rod and vaporization at the pellet surface is discussed, showing that it could explain the pronounced swelling of the fuel pellet reported from PIE.

Keywords: PWR, power ramp, fuel melting, simulation, Post-Irradiation Examinations

I. Introduction

The Power to Melt and Maneuverability (P2M) project, proposed within the OECD/NEA Framework for IrraDiation ExperimentS (FIDES [1][2]) by the Nuclear Research Center (SCK·CEN, Belgium), the Commissariat à l'Énergie Atomique et aux Énergies Alternatives (CEA, France) and Électricité de France (EdF, France), aims at studying the behavior of Light Water Reactor (LWR) high burnup fuel during slow power transients up to fuel centerline melting. Staircase power ramps are planned in the BR2 reactor [3] (Belgium) to avoid failure of the cladding

*Corresponding author.
Email address: jerome.sercombe@cea.fr (J. Sercombe)

by Iodine Stress Corrosion Cracking (I-SCC) during the transients.

In 2021, an international Simulation Exercise (SE) on past fuel melting experiments was organized within the P2M project in order to calibrate fuel performance codes on past power ramps during which fuel melting took place [4][5]. Among the two test cases considered for the SE, the HBC-4 fast power ramp (72 $kW.m^{-1}.min^{-1}$) was performed on high burnup fuel (60 $GWd.tU^{-1}$ at Peak Power Node) up to a RTL of 66 $kW.m^{-1}$, as obtained by gamma spectrometry, 70 $kW.m^{-1}$, according to online measurements of thermal fluxes during the test. In the P2M Simulation Exercise, it was decided to consider the lowest value as the reference and include calculations with the estimated ± 7% power uncertainty to cover the highest value. According to the Post Irradiation Examination (PIE) of the rod [6][7], fuel centerline melting and fuel relocation took place, indicating that the liquidus was reached during the test. Failure of the cladding by I-SCC was also reported at six axial locations around the PPN. In some of the ceramographies, clad failure, central holes, fuel melting and extensive fuel expansion were observed.

To the authors knowledge, the impact of I-SCC clad failure on the fuel deformation, temperature and potential melting has been little studied. On the contrary, the impact of water ingress in CANDU fuel rods following clad failure by I-SCC has been extensively studied by Lewis et al. [8][9] to estimate the release of Fission Products (FP) in the coolant. The modeling of fuel oxidation by water vapor in defective CANDU fuel was later considered by Lewis et al. [10][11] and Higgs et al. [12] since it can alter significantly the thermal conductivity of the fuel and therefore increase the fuel centerline temperature. During the high power operating conditions specific to CANDU reactors, fuel melting has been observed in defective fuel rods at power levels lower than expected. Welland and al. [13] developed a phase field model of incipient melting in defective fuel where thermal heat transport is coupled to oxygen transport. This approach confirmed the deleterious impact of fuel oxidation on the power-to-melt of unirradiated fuel in CANDU reactors.

The Simulation Exercise was limited to 1.5D simulations of the HBC-4 fuel melting experiment, as detailed in D'Ambrosi et al. [4][5]. To investigate the (potential) impact of clad failure on fuel melting, 2D(r,θ) simulations of this experiment with the fuel performance code ALCYONE are proposed in this paper. The 2D(r,θ) scheme is first described in section II together with the thermodynamic based modeling of fuel melting available in ALCYONE. The main characteristics of the HBC-4 power ramp are then briefly recalled in section III. Simulations results with and without clad failure are then presented in section IV. An extensive discussion of the results including the impact of water ingress and of fuel oxidation by steam is then proposed in section V.

II. The 2D(r,θ) schemes of ALCYONE

ALCYONE is the fuel performance code dedicated to PWR fuels developed by the CEA, EdF and FRAMATOME within the PLEIADES computational environment [14][15][16]. The latest version (ALCYONE V2.1 [17]) includes three different schemes that provide a description of the complete fuel rod behavior (1.5D scheme) or of the local behavior at a given axial position in the rod (2D(r,θ) [18] or 3D [19] schemes). A 1.5D simulation of the fuel rod behavior during the power transient and the base irradiation that preceeds is a necessary step before performing 2D(r,θ) or 3D local simulations. The local power history, the rod internal pressure history and

the local clad external temperature history are obtained from the 1.5D simulation and used as inputs in the 2D(r,θ) and 3D simulations. The 1.5D simulation results of the HBC-4 experiment and of the base irradiation in the BR3 reactor are described in D'Ambrosi et al. [4] and will not be detailed here. They have been used to generate the data files of the 2D(r,θ) simulations of this paper.

II.A. Standard 2D(r,θ) scheme

ALCYONE V2.1 includes by default a 2D(r,θ) generalized plane strain[1] scheme, specifically developed for Pellet Cladding Interaction (PCI) studies [18]. The scheme describes the behavior of a fuel rod containing pellets initially fractured in eight identical fragments (based on the observed crack pattern of fuel pellets after base irradiation in PWR). Due to the symmetry conditions, only half of a pellet fragment (vertex angle of 22.5°) and the overlying cladding are meshed, as illustrated in Figure 1.

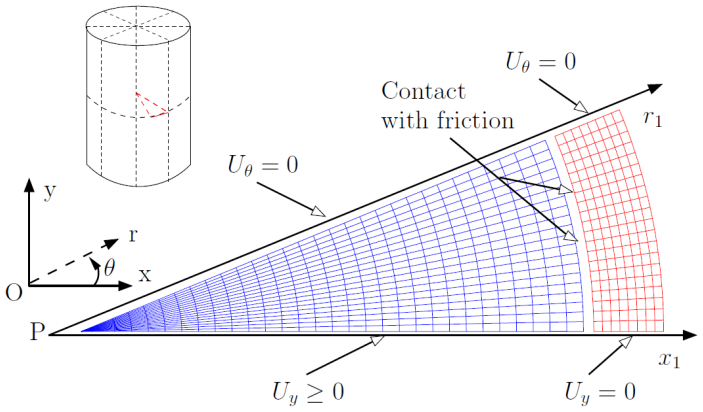

Figure 1: Mesh and boundary conditions in ALCYONE 2D(r,θ) standard scheme (reproduced from [18]).

The mechanical boundary conditions reflect the pellet fragmentation with the symmetry plane of the fragment ($U_\theta = 0$) on (Pr_1) and the fracture plane on (Px_1) where the vertical displacement $U_y \geq 0$ is not known a priori but depends on the loading conditions of the fuel. For the cladding, symmetry conditions ($U_\theta = 0$) are prescribed on the same planes. Unilateral contact with friction is considered at the pellet clad interface since it greatly modifies the stress distribution in the cladding and the secondary cracking of the fuel pellet (i.e., the cracks that develop during a power transient). More details on this aspect can be found in Sercombe et al. [18].

The thermal boundary conditions are somehow disconnected from the mechanical boundary conditions. The temperature history of the clad outer surface obtained from the 1.5D simulation at the axial position of interest in the rod is prescribed in the 2D(r,θ) calculation (i.e., there is no evaluation of the coolant thermal-hydraulics in 2D(r,θ)). Heat transfers between adjacent fuel

[1] Realistic out-of-plane stresses and strains are included in the analysis

pellet fragments (i.e., in the fuel pellet radial cracks) are furthermore neglected (i.e., a zero heat flux is prescribed on the symmetry and fracture planes of the fragment). This condition leads a temperature distribution in the pellet fragment that is very close to the radial profile of the 1.5D simulation.

The thermal and mechanical models used in the 2D(r,θ) simulations are as in the 1.5D simulation of the fuel rod. Fuel secondary cracking and thermal creep, fission gas induced swelling and release [20], fuel densification and solid swelling, clad irradiation and thermal creep, clad plasticity are all part of the physical models considered in the simulations. Details can be found in Sercombe et al. [15][18]. For this reason, very close results (temperature distribution, fuel and clad average deformation) are obtained with the 1.5D and 2D(r,θ) schemes. The 2D(r,θ) scheme does however provide the stress localization in the cladding expected in front of an opening pellet radial crack [21].

II.B. Multi-fragment 2D(r,θ) scheme for clad failure

Simulation of clad failure is not possible with the standard 2D(r,θ) scheme of ALCYONE. The modeling of the partial failure of the cladding during Reactivity Initiated Accidents (RIA) has however been reported by Sercombe et al. [22]. In this work, the brittle failure of a hydride blister extending over 50 % of the cladding thickness was assumed to occur when the hoop stress at the clad outer wall reached a specific level. It was shown that this partial failure led to the reopening of the pellet-clad gap below the partially cracked cladding and to the local bending of the cladding. The standard 2D(r,θ) configuration is however not realistic when a through-wall crack forms in the cladding. For this reason, a multi-fragment 2D(r,θ) scheme has been developed in ALCYONE. It is described in Figure 2.

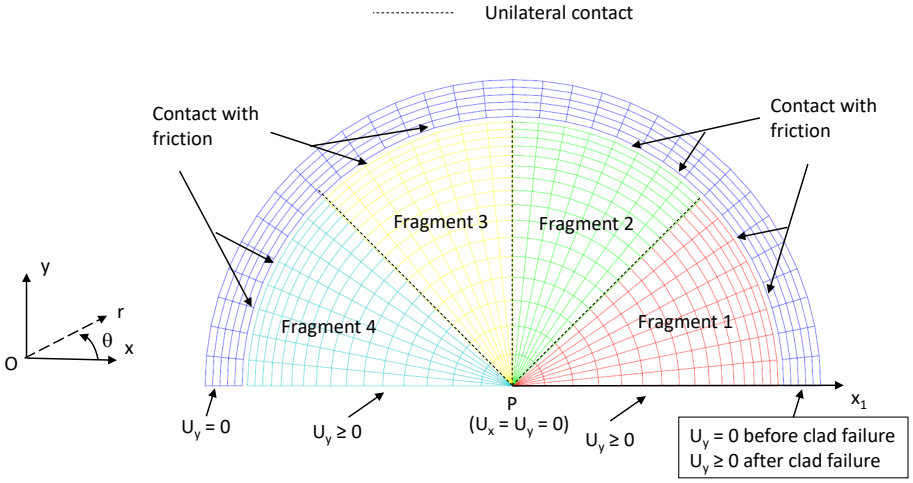

Figure 2: Mesh and boundary conditions in ALCYONE 2D(r,θ) multi-fragment scheme.

Compared to Figure 1, half of the fragmented pellet and of the overlying cladding is this time considered in the simulation. Four identical fragments with a vertex angle of 45° are meshed.

The mechanical boundary conditions are chosen to match those of the standard 2D(r,θ) scheme. Fracture planes are introduced on the (Px_1) plane: $U_y \geq 0$ for fragment 1 and 4. Unilateral contact conditions are introduced at the fragment - fragment interfaces to avoid interpenetration (marked by the dashed black lines). As in the standard 2D(r,θ) scheme of ALCYONE, unilateral contact with friction is considered at the pellet fragments - clad interface.

Concerning the thermal boundary conditions, very high heat fluxes are considered at the fragment - fragment interfaces to avoid marked discontinuities on the radial temperature profiles between fragments. This might be a strong hypothesis but it has been adopted since a proper heat transfer coefficient - pellet crack opening function is not available at present. The remaining boundary conditions are similar to those considered in the standard 2D(r,θ) scheme: prescribed temperature on the clad outer wall, zero heat flux on plane (Px_1). It is thus implicitely assumed that the clad to coolant heat exchanges are not significantly modified by the failure of the rod. This is related to the small change in rod geometry induced by the I-SCC failure of the cladding.

During base irradiation and at the beginning of the power transient, the mechanical boundary conditions reflect the integrity of the cladding with symmetry conditions on the plane (Px_1): $U_y = 0$ on the clad walls situated in front of fragments 1 and 4. The progressive failure of the cladding by I-SCC is then represented by a time-dependent relaxation of the $U_y = 0$ boundary condition on the plane (Px_1) in front of fragment 1. The following function is used:

$$f(t) = \frac{(t - t_0)}{(t_f - t_0)} \quad \text{if} \quad t_0 \leq t \leq t_f \tag{1}$$

where $f(t)$ is the fraction of the cladding thickness that is cracked at time t, t_0 the crack initiation time on the inner clad wall and t_f, the time when a through-wall crack is found. At each time t, all the cladding nodes on plane (Px_1) that are located between $x = R_i$ and $x = R_i + f(t) \times e$ with R_i the clad inner radius and e the cladding thickness, are free to move upward ($U_y \geq 0$). When a through-wall crack is formed (at $t = t_f$), the internal rod conditions are changed as follows: the rod internal pressure is set equal to the external coolant pressure and applied on all the fragment surfaces and internal clad wall; the rod internal composition is modified assuming that all the gases are replaced by water vapor. The URGAP model is used in ALCYONE to estimate the heat exchange coefficient at the pellet-clad interface [23]. In theory, water ingress in the rod can lead to a substancial decrease of the heat exchange coefficient due to the five times lower thermal conductivity of water vapor (0.06 $W.m^{-1}.K^{-1}$ at 700 K) compared to that of He filling the non irradiated rod (0.28 $W.m^{-1}.K^{-1}$ at 700 K).

Verification of the multi-fragment 2D(r,θ) scheme was done by comparing the results of the calculation without clad failure to those obtained from the standard 2D(r,θ) scheme: the fuel centerline temperature, the fuel radius, the clad outer radius and the Fission Gas Release (FGR) were checked, showing the good behavior of the multi-fragment 2D(r,θ) scheme.

II.C. Thermodynamic based modeling of fuel melting

The assessment of fuel melting being the primary goal of the P2M project, an advanced model has been implemented in ALCYONE. It relies on thermodynamic equilibrium calculations of the complex system at hand in irradiated fuel. The Fission Products (FP) and actinides considered in the calculations are given in Table I.

To reduce the size of the system to 14 representative elements (He, U, Pu, Ba, Zr, Cs, I, Te, Mo, Ru, Pd, Cd, La, Gd) plus oxygen (the non irradiated fuel is assumed at stoichiometry), the FP and actinides that have a similar chemical behavior (e.g., high solubility in the fuel, found mostly in metallic form, ...) are grouped together. The quantity of each element is estimated with the neutronics based solver PRODHEL integrated in ALCYONE [24]. The inventory includes only the long-lived FP obtained after an irradiation at a fixed power (20 $kW.m^{-1}$) up to an average fuel burnup of 10 to 80 $GWd.tU^{-1}$.

He	**U**	**Pu**	**O**	**Ba**	**Zr**	**Cs**	**I**	**Te**	**Mo**	**Ru**	**Pd**	**Ce**	**La**	**Gd**
Xe	U	Pu	O	Ba	Zr	Cs	I	Te	Mo	Ru	Pd	Ce	La	Eu
Kr		Np		Sr	Nb	Rb	Br	Se		Tc	Sn	Pr	Y	Sm
He		Am						Ge		Rh	Sb			Gm
		Cm						As						Nd
														Pm

Table I: Fission Products and actinides considered in the thermochemical equilibrium calculations. The first line gives the representative element.

Thermodynamic equilibrium calculations have been performed using the open-source software OpenCalphad [25][26] integrated in ALCYONE [27] and the Thermodynamics of Advanced Fuels International Database [28][29] (TAF-ID). The latter includes a sophisticated thermodynamic model to describe the fluorite phase U-Pu-O-FP where the solubility of some FP (Ce, Gd, La, Nd, Np, Pu, Zr) is taken into account. The TAF-ID relies on the Calphad method and is therefore well suited to evaluate the melting of the fluorite phase. In this respect, numerous experimental data on U-O and U-Pu-O melting are used to build the models and ensure therefore a precise assessment of the solidus and liquidus as a function of the stoichiometry deviation of the fuel [30][31].

The results from the thermodynamic equilibrium calculations are summarized in Figure 3. The evolution of the fuel liquid fraction (i.e., the moles of elements in the liquid phase divided by the total number of moles) as a function of temperature is given for different fuel average burnups. Each curve is characterized by a negligible liquid fraction up to a temperature of $\sim$ 2600°C. The non zero liquid fraction before this temperature reflects the formation of secondary liquid stoichiometric phases in small quantities such as $CsI_{(l)}$, $Cs_2MoO_{4(l)}$, ... At a given temperature threshold corresponding to the melting of the fluorite phase, a slow increase of the liquid fraction takes place followed by a sharp increase. The temperature at which the liquid fraction reaches one is the liquidus. The temperature corresponding to the melting of the fluorite phase is the solidus. Irrespective of the fuel average burnup, it starts when the liquid fraction reaches $\sim$ 10 %. The curves of Figure 3 illustrate the impact of FP on melting with a decrease of the solidus and liquidus temperatures with the average burnup, as expected from available measurements [32][33]. Thermodynamic equilibrium calculations provide also the evolution of the fuel enthalpy from which the heat capacity can be derived. The evolution of the latter with temperature is plotted in Figure 4 for different fuel average burnups.

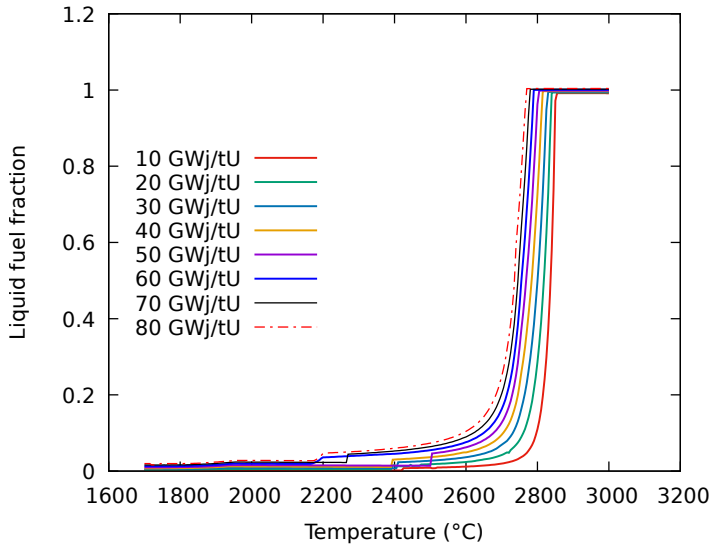

Figure 3: Calculated evolution of the fuel liquid fraction with temperature and fuel average burnup

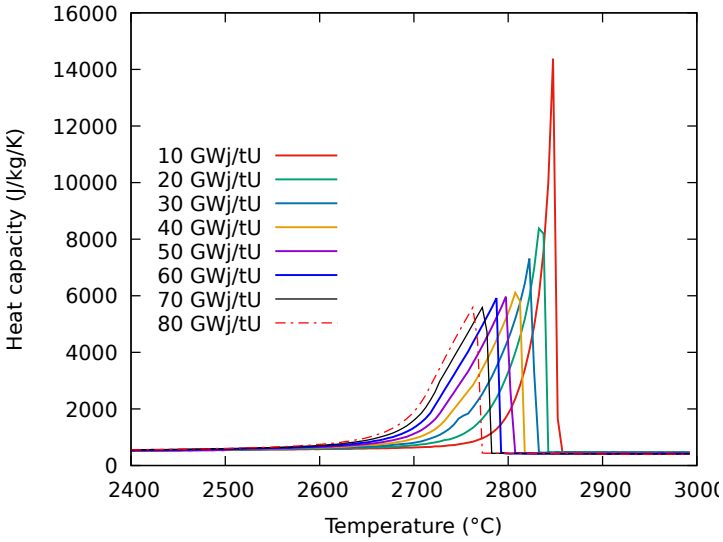

Figure 4: Calculated evolution of the fuel heat capacity with temperature and fuel average burnup

The trend with burnup follows that of the liquid fraction with a decrease of the magnitude of the peak observed upon melting (i.e., corresponding to the latent heat of melting) and a shift of the curves towards lower temperatures. In the proposed application to the HBC-4 power ramp and since only the PPN is of interest, the fuel liquid fraction and the heat capacity curves corresponding to an average burnup of 60 GWd.tU^{-1} are used in ALCYONE. According to the thermodynamic calculations, the solidus is reached at 2645 °C and the liquidus at 2790 °C.

Several thermo-mechanical models have furthermore been adapted to account for fuel melting. The thermal conductivity of the fuel, the elastic and shear moduli, the thermal expansion of the fuel have been made dependent on the fuel liquid fraction using a simple mixing law. This allows a continuous description in case of phase change. Furthermore, the fuel thermal expansion model includes the 9.6 % volume change associated to fuel melting. More details can be found in D'Ambrosi et al. [34] where the same methodology was applied to a fuel of average burnup 30 GWd.tU^{-1}.

III. Main characteristics of the HBC4 power ramp

A short description of the HBC-4 power ramp is here provided. The irradiation sequence that took place before the power transient is not detailed. PIE of importance for the present 2D(r,θ) simulations are detailed. A complete description of the HBC-4 fuel rod, loading histories and of the available PIE is proposed in D'Ambrosi et al. [4] and Bonny et al. [7], based on the report of Blanpain [6]. Readers may refer to these papers for more information.

III.A. Power history and clad failure

The power or Linear Heat Generation Rate (LHGR) history at PPN during the last part of the HBC-4 experiment is plotted in Figure 5. Note that the time equal to zero refers to the time when the RTL is first reached. The irradiation consisted first in a gradual and slow power increase by steps of 5 kW.m^{-1} up to the preconditioning level of $\sim$ 37-41 kW.m^{-1} (not shown in Figure 5). After 20 h, the power was raised in $\sim$ 30 s till an estimated 66.3 $\pm$ 4.6 kW.m^{-1}. This power was then maintained during 40 s and then decreased to 10 kW.m^{-1} in 60 s. During the test, the radiation detector located along the sampling line gave no sign of fuel rod damage and Fission Product (FP) release in the loop. During the depressurization of the rig, a considerable rise in activity was measured, indicating that the cladding had failed. The timing of the failure in hot conditions was however ascertained later by microstructural examinations. Note that the 66.3 $\pm$ 4.6 kW.m^{-1} LHGR at RTL is based on the measured axial profile of Zr activity by gamma spectrometry after the power ramp. On-line measurements of the thermal fluxes in the testing loop have led to a calculated LHGR of 70 $\pm$ 7.1 kW.m^{-1}. In the P2M simulation exercise [4], it was decided to consider the 66 kW.m^{-1} as a reference and include simulations with a $\pm$ 7% power uncertainty to cover the highest estimate.

In this work, to model clad failure, it has been assumed that crack propagation is initiated at t_0 = 0 s and proceeds until t_f = 30 s where a through-wall crack is formed. The failure time indicated in Figure 5 (30 s) is indicative but consistent with the late release of FP in the coolant. Failure times by I-SCC during straight power ramps performed in the OSIRIS reactor in France have been reported by Mougel et al. [35], based on FP release detection in the test loop, and analyzed later by Sercombe et al. [36]. It was found that the failure time decreases

with the power increase step (ΔP = 15 to 40 kW.m^{-1}) and reaches a lower limit of ~ 100 s at a ΔP of 25 kW.m^{-1}. The 30 seconds considered in the HBC-4 simulation are therefore below the measured failure times in the OSIRIS reactor. Several reasons might explain this fast failure of the cladding. First, the power increase rate in the HBC-4 power ramp is much higher than in all the OSIRIS ramps (72 kW.m^{-1}.min^{-1} compared to 10 kW.m^{-1}.min^{-1}). Second, the RTL and the fuel average burnup are extremely high ($\geq$ 66 kW.m^{-1} and 60 GWd.tU^{-1}), which are not common conditions. These conditions have certainly led to higher than usual temperatures of the clad inner wall. Since temperature is a very important factor with respect to I-SCC kinetics [37], this might explain the fast failure of the cladding during the HBC-4 power ramp.

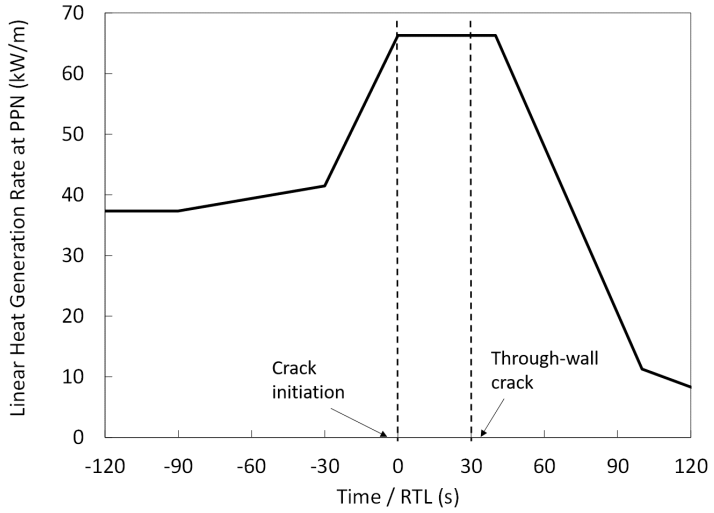

Figure 5: Power history at PPN during the HBC-4 fast transient

III.B. PIE

Figure 6 presents the clad diameter axial profile (black line) in the vicinity of the PPN, together with the normalized axial power profile (red line). The clad diameter profile presents six peaks that mark the position of the cracks in the cladding. While the diameter in the non cracked regions is close to 9.5 mm, it reaches 9.8-10 mm in front of the clad cracks. The axial power profile presents a marked evolution along the rod that is characteristic of reactor irradiation in BR2. The location of the main central holes detected by neutron radiography are also indicated in Figure 6. They have been confirmed by the observations of the transverse (CT1, CT2) or longitudinal (CL1) ceramographies performed at the same axial positions. A third transverse ceramography was performed outside of the failed cladding region (CT3). The CT1, CT2 and CT3 transverse ceramographies are presented in Figure 7.

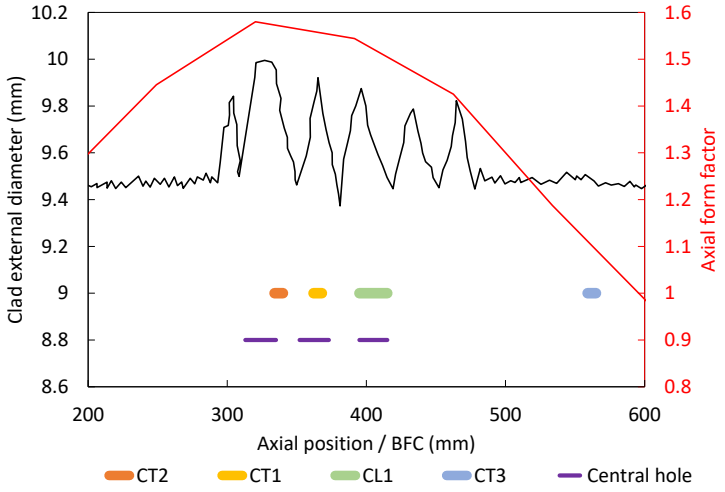

Figure 6: Clad diameter axial profile (black line) after the HBC-4 power ramp, axial power profile (red line) and axial location of the ceramographies and of the central voids (arbitrary vertical position in the graph).

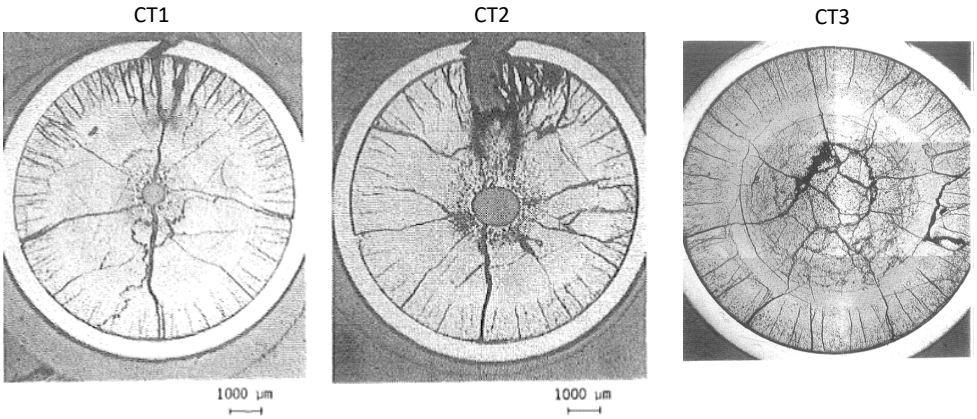

Figure 7: Ceramographies performed after the HBC-4 power ramp.

The CT1 and CT2 ceramographies confirmed the presence of central voids and of through-wall cracks in the cladding that showed the characteristic pattern of I-SCC with a bifurcation halfway through the clad thickness (slow crack propagation by I-SCC followed by a low ductile failure of the remaining clad ligament). The roundness of the central void is clear in the CT1 cross-section while it has an elliptic shape in the case of CT2 with the smallest dimension aligned with the clad crack. The fuel swelling is also markedly more important in the direction of the clad crack since no reopening of the pellet-clad gap is visible. This results in a central hole that appears shifted away from the clad crack. On the contrary, due to the lower local LHGR (56 $kW.m^{-1}$), CT3 presents no central void and no crack in the cladding. One important fea-

ture that was reported is the axial discontinuity of the central holes, separated by regions filled with molten fuel. This clearly indicated that the central holes were not a consequence of the well-known pore migration mechanism triggered by the temperature gradient that takes place in Sodium Fast Reactor fuels [38] but rather of fuel melting. The reason being that the short holding time at RTL was probably not sufficient to activate significant pore migration. The melt diameters were estimated at 1.6 mm in CT1 and 2.2 mm in CT2, based on the size of the dense fuel ring with numerous pear-shaped and spherical pores that surrounds the central holes. These melt diameters are somehow consistent with the size of the central holes (0.7 mm in CT1 and 1.2 mm in CT2) if one considers that the latter are formed by shrinkage of the once molten fuel upon cooling down [39] and slightly increased by fuel relocation. The longitudinal cross-section and a more in-depth discussion of the melted fuel microstructure can be found in [4] and [7].

IV. Simulation results

Simulation results obtained with the 2D(r,θ) multi-fragment scheme accounting or not for clad failure are presented to illustrate the impact of clad failure on the fuel deformation, temperature and melting. Note that the results obtained with the 2D(r,θ) scheme without clad failure are very close to the simulation results of the 1.5D scheme concerning the slice located at PPN. These results are detailed in D'Ambrosi et al. [4] and will not be recalled here.

IV.A. Clad failure

Figure 8 gives the evolution of the calculated clad external diameter situated on the (Px_1) axis in the multi-fragment 2D(r,θ) simulations with and without clad failure. The LHGR evolution is also given in the figure.

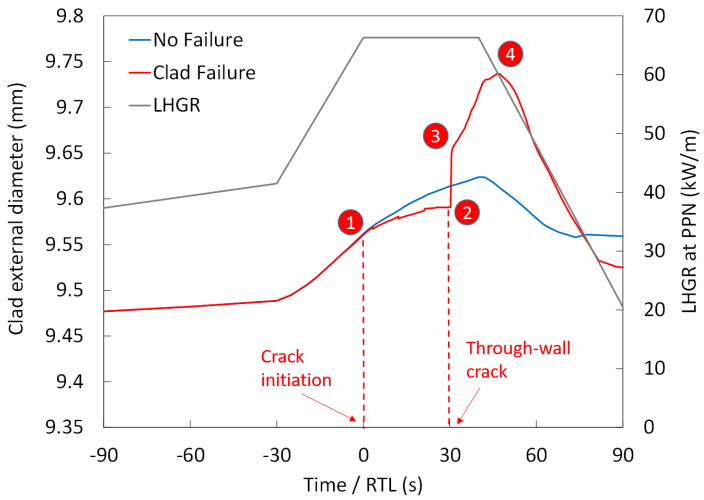

Figure 8: Calculated evolution of the clad diameter in the multi-fragment 2D(r,θ) simulations with and without clad failure.

During the power transient (-30 to 0 s), the clad diameter in the 2D(r,θ) calculation without clad failure increases regularly (see the blue curve). A maximum is reached at the end of the

holding period at RTL (40 s). In the 2D(r,θ) calculation with clad failure, crack propagation is initiated at t_0 = 0 s (time 1) and proceeds until t_f = 30 s (time 2) where a through-wall crack is formed. The crack propagation kinetics is given by equation 1 and illustrated in Figure 9. The colors indicate the temperature distribution in the fuel pellet. To give a full picture of the pellet state, the simulated half pellet is duplicated by symmetry along the (Px_1) axis.

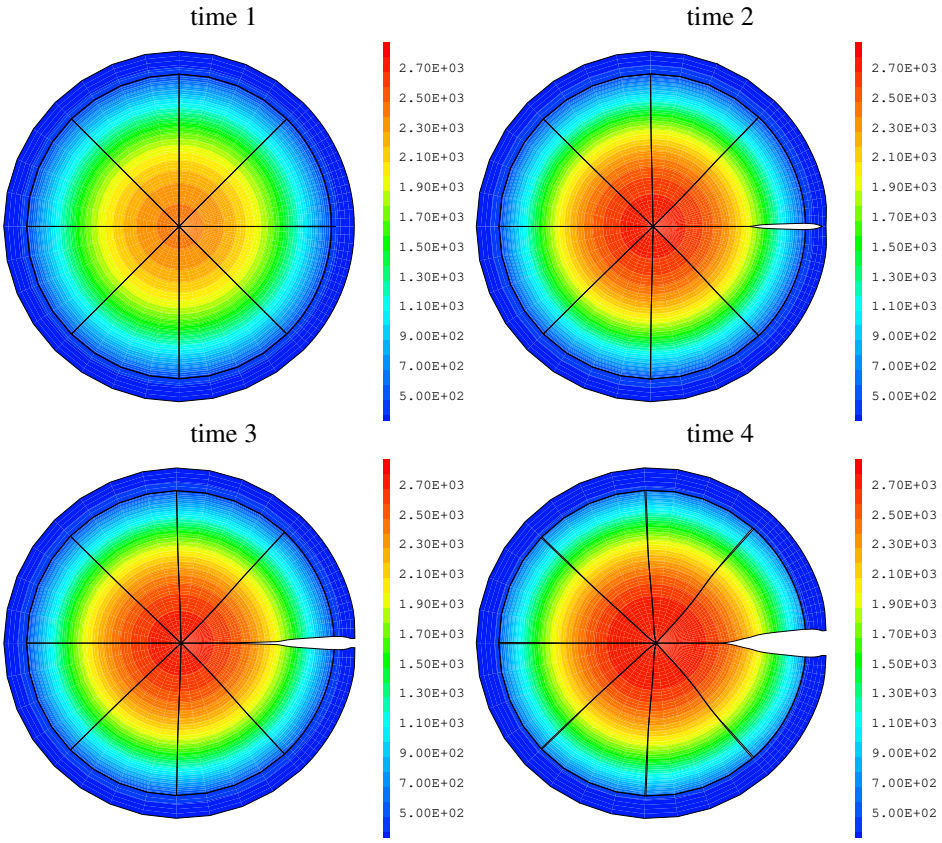

Figure 9: Simulation of clad failure with the multi-fragment 2D(r,θ) scheme: time 1, crack initiation at the inner clad wall at t = 0 s; time 2, crack propagation with contraction of the clad outer wall (necking) at t = 30 s; time 3, through-wall crack at t = 30.6 s; time 4, maximum crack opening at t = 48 s. The scales and the colors show the temperature distribution in °C.

As can be seen in Figure 8, the crack propagation phase (time 1 to 2) leads to a decrease of the clad diameter when compared to the calculation without clad failure. This is due to the slow propagation of the crack in the clad thickness that takes place when the cladding is loaded by the expanding fuel pellet. It leads to a plastic strain localization in the non cracked clad ligament that is characterized by a pronounced necking, see Figure 9. Between times 2 (t = 30 s) and 3 (t = 30.6 s), the development of a through-wall crack leads to a sudden increase of the clad external diameter (by 0.05 mm). Between times 3 (t = 30.6 s) and 4 (t = 48 s), the clad diameter increases rapidly due to the expanding fuel pellet that is no more restrained by the cladding. The clad diameter reaches a maximum of 9.73 mm to be compared with the 9.62 mm when clad failure

is not considered. In the 2D(r,θ) calculation without failure, the end of the holding period at RTL (t = 40 s) marks the beginning of the decrease of the clad diameter. This is not the case in the 2D(r,θ) calculation with clad failure where the momentum up to t = 40 s is kept during the next few seconds in spite of the decreasing LHGR. The pace of the increasing clad diameter is however reduced during this time period (t = 40 to 48 s).

The evolution of the clad crack opening during the power ramp is plotted in Figure 10. It reaches a maximum of 0.7 mm at t = 48 s. The return to cold state leads to a partial closing of the crack with a residual value of 0.3 mm (not shown on the graph). Note that the high friction coefficient at the pellet-clad interface leads to a clad crack opening that follows the pellet radial crack opening (see time 4 in Figure 9). In ALCYONE, the friction coefficient increases with the burnup of the fuel, as detailed in Sercombe et al. [18].

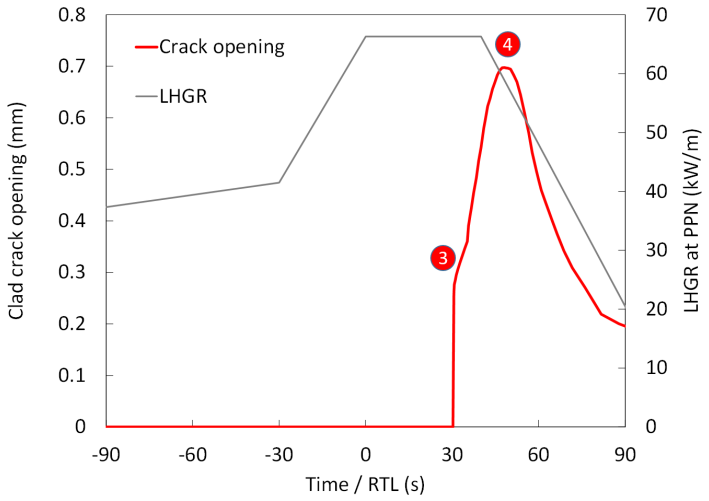

Figure 10: Calculated evolution of the clad crack opening in the multi-fragment 2D(r,θ) simulation

IV.B. Fuel temperature and melting

The evolutions of the calculated fuel temperatures at the pellet center in the multi-fragment 2D(r,θ) simulations with and without clad failure are given in Figure 11. As can be seen, equivalent temperatures are obtained in the two simulations up to t = 0 s (time 1). A small difference is then observed due to the propagation of the crack in the clad thickness (5 °C at t = 30 s). When the through-wall crack is formed at t = 30.6 s (time 3), the temperature rises in the calculation and reaches a maximum of 2801 °C that can be compared to the 2761 °C in the calculation with no failure of the cladding. This small temperature difference (40 °C) is due to the increase of the pellet diameter that results from the loss of rigidity of the cladding and to the replacement of He in the rod by water vapor that degrades the heat exchange coefficient at the pellet-clad interface. As for the clad diameter, the temperature continues increasing during the first few seconds that follow the end of the holding period at RTL (t = 40 to 48 s) in spite of the decreasing LHGR. This shows that thermal equilibrium has not been reached following clad failure.

The maximum liquid fuel fractions calculated during the multi-fragment 2D(r,θ) simulations with and without clad failure are shown in Figure 12. As was expected from the calculated temperatures, the liquidus is reached at the pellet center in the calculation with clad failure while the liquid fuel fraction does not exceed 0.7 in the calculation without failure.

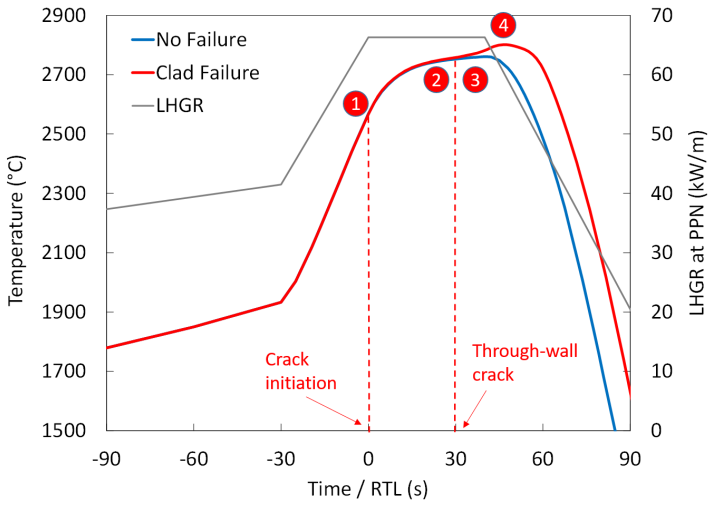

Figure 11: Calculated evolution of the fuel temperature at the pellet center in the multi-fragment 2D(r,θ) simulations with or without clad failure

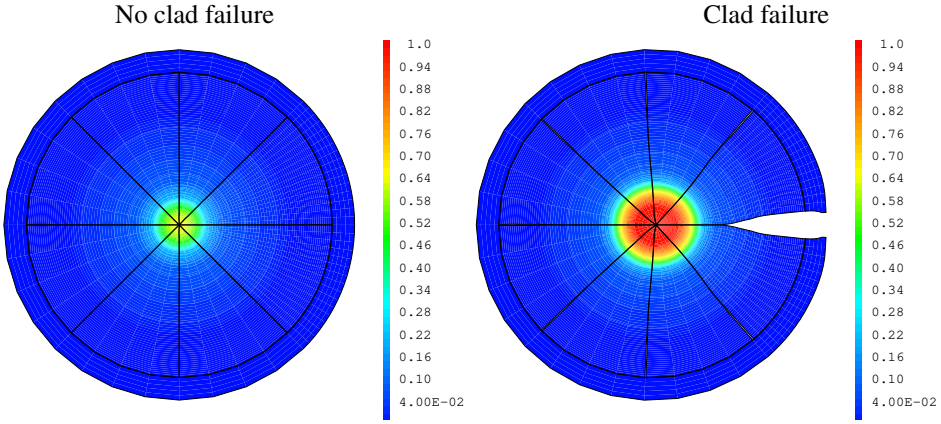

Figure 12: Calculated maximum liquid fuel fractions during the multi-fragment 2D(r,θ) simulations with or without clad failure

The radial profiles of the liquid fuel fraction at t = 48 s (time 4) in the four pellet fragments are plotted in Figure 13. According to the calculated profiles, the completely melted fuel region (liquid fuel fraction equal to 1) extends up to a radius of 0.5 mm. The solidus (corresponding to a liquid fuel fraction of 0.1) is reached at a radius of 1.4 to 1.5 mm. The radial extension of

the liquid fuel fraction is slightly affected by the clad crack opening. Fragment 1 presents the highest liquid fuel fractions at all radial positions. Consistent with this result, a small dissymetry appears in the maximum fuel diameters with a greater diameter in the (Px1) plane aligned with the clad crack (8.537 mm) compared to the one in the perpendicular direction (8.507 mm). This leads to a small excentricity of the hot fuel pellet center in the direction of the clad crack (see the apparent radial displacement of the pellet center in Figure 12) that reaches a maximum of 0.13 mm at time 4. In spite of this small dissymetry, the central melted zone remains very close to circular with no marked influence of the clad crack.

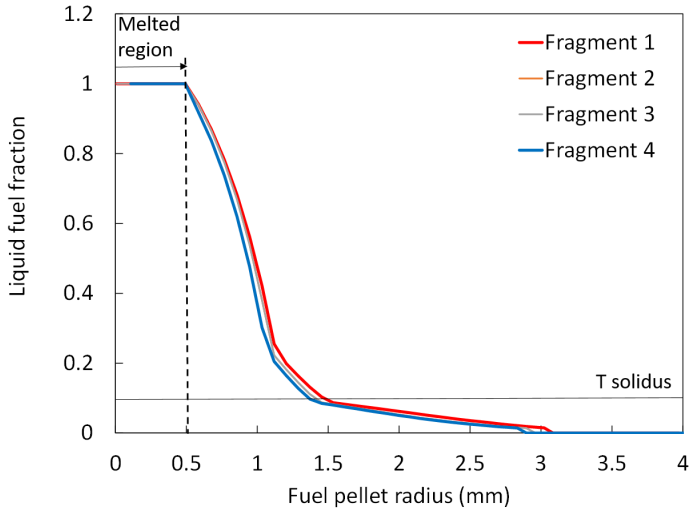

Figure 13: Calculated radial profiles of the fuel liquid fraction in the four fragments of the 2D(r,θ) simulation with clad failure

V. Discussion

Simulation results can be compared to the available PIE. A refined analysis of the CT1 cross-section is first proposed to better assess the simulation results. The ceramography at the location of CT1 is preferred to CT2 because the clad defect is less developed and one can expect less consequences related to water ingress. This corresponds better with the 2D(r,θ) simulations of this paper where only thermomechanical aspects related to clad failure have been studied. Figure 14 presents the CT1 cross-section with a zoom on the fuel pellet center and the clad crack. It must be emphasized that the ceramography is of poor quality which leads to some non negligible uncertainties in the determination of the different measures proposed hereafter. To reduce uncertainty as much as possible, measurements have been made manually on 20 cm x 30 cm prints of the ceramographies.

The magnification led to the estimation of the pellet center position (intersection of the red lines) that does not correspond with the center of the central hole. The latter appears shifted in the direction of the clad crack. The radial shift is small and estimated at 0.15 mm. The central

hole is close to circular with an estimated diameter of 0.7 mm. The magnification of the central part of the pellet shows the existence of a dense fuel layer with numerous large pores surrounding the central hole. As discussed by Blanpain [6] and D'Ambrosi et al. [4], this dense layer can also be associated with fuel melting. The dense layer thickness is not homogeneous but slightly more important in the direction of the clad crack. Overall, the melted fuel diameter reaches ~ 1.6 mm. From Figure 14, the residual clad crack opening can be estimated at ~ 0.35-0.54 mm, depending on the radial position in the clad wall.

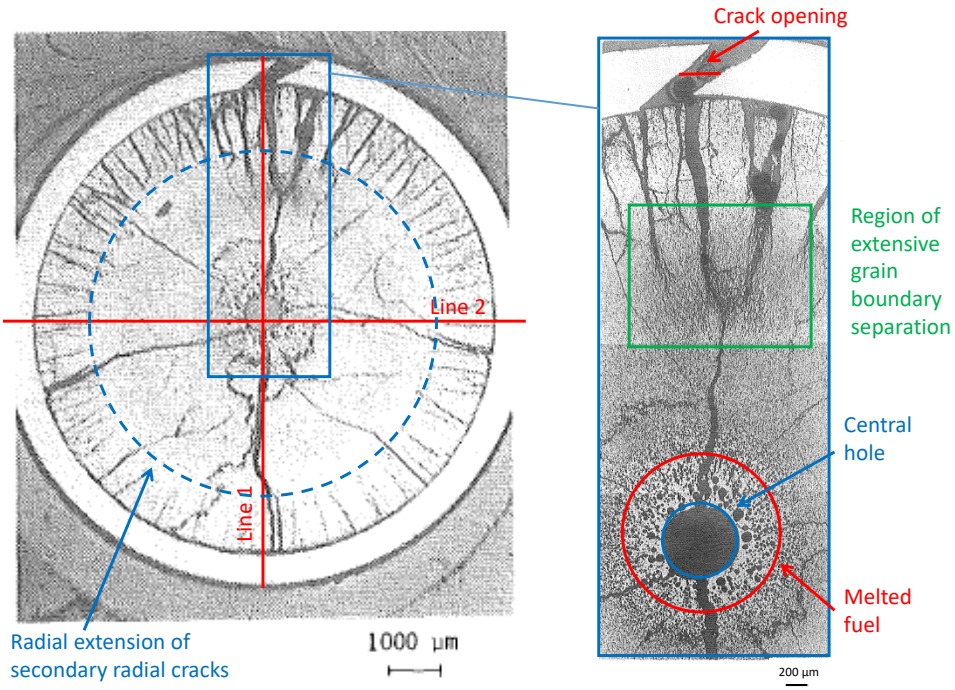

Figure 14: CT1 cross-section with a zoom showing the central hole, the dense fuel layer surrounding it, the region where extensive grain boundary separation is visible and the clad crack.

The mesh size of the 2D(r,θ) simulations at the pellet center in the radial direction being of 0.1 mm, the melt diameter can only be estimated with a similar precision. If a fuel liquid fraction of 1 is considered as an indicator of fuel melting, the calculated melted fuel diameter equals 1 mm (see Figure 13), which is smaller than the measured diameter from the CT1 cross-section based on the boundary of the dense fuel layer (1.6 mm). The 1.6 mm diameter corresponds to a calculated liquid fuel fraction of ~ 0.8 (see Figure 13). Since this value remains close to 1, it is possible that the estimated melt diameter includes a small proportion of nearly molten fuel close to the boundary. This might explain the underestimation of the melted fuel diameter. A small excentricity of the melted fuel region in the direction of the clad crack is visible in the 2D(r,θ) simulation, see Figure 9, with a maximum offset of 0.13 mm, to be compared with the measured 0.15 mm.

The 2D(r,θ) simulation underestimates the residual clad crack opening (0.3 mm compared to the measured 0.3-0.54 mm). It must be recalled that the 2D(r,θ) configuration is based on the assumption that the simulated crack is infinite in the out-of-plane direction. In reality, the axial extension of the crack is limited to a few milimeters and might present extensive plastic strains at the crack tips that could hinder the closing of the crack upon unloading. This might explain the obtained discrepancy. Another reason could be the underestimation of the pellet fragment swelling, as discussed in the next paragraphs.

The CT1 cross-section of Figure 14 can also be used to give rough estimates of the fuel and clad diameters in the plane of the clad crack (red line 1) and perpendicular to the plane of the clad crack (red line 2). The fuel pellet diameter along line 1 is equal to $\sim$ 8.7 mm, while it is equal to $\sim$ 8.52 mm along line 2. Considering the pre-ramp fuel pellet diameter of 8.2 mm, this leads to a maximum fuel expansion of $\sim$ 6 %. The clad diameter along line 1 is somehow equal to the clad diameter along line 2 ($\sim$ 9.81 mm). This shows that the residual strain in the cladding is uniform along the circonference, which is characteristic of a brittle failure by I-SCC.

The calculated fuel pellet diameters at cold state are 8.238 mm and 8.27 mm along lines 1 and 2, respectively. On average, they indicate a fuel pellet swelling of 2.6 %, far from the measured 6 %. Note that the fuel pellet swelling in the CT3 ceramography (no fuel melting) was estimated at 2% [6], in relative agreement with the calculation proposed here for CT1. It must be recalled that the modeling of melting in ALCYONE accounts for the 9.6 % volume expansion related to the phase change. The calculated versus measured difference in the fuel pellet swelling could be due to the numerous secondary radial cracks that can be seen at the pellet periphery, see the CT1 ceramography of Figure 14. As illustrated by Figure 15 where the calculated fuel pellet radial cracking at t = 30 s in Fragment 1 is plotted, ALCYONE includes a fuel pellet mechanical model that describes the development of secondary radial cracks during the power ramp [18][40]. Note that the radial extension of the secondary cracks is fairly consistent with those of the CT1 ceramography ($\sim$ 1 mm, see Figure 14). However, in this model, reversibility of the pellet radial crack opening is assumed which means that the pellet secondary cracks will disappear completly at cold state. This might explain the underestimation of the apparent fuel pellet volume.

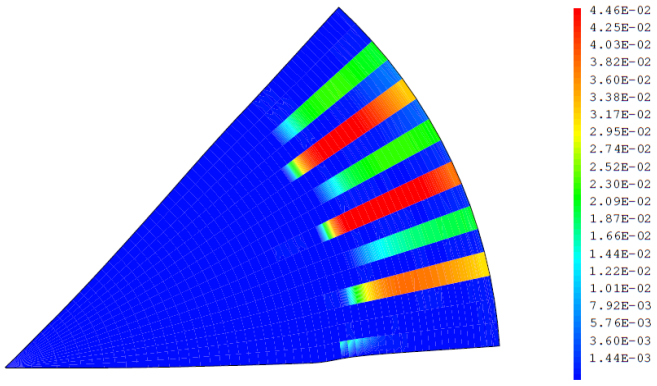

Figure 15: Calculated secondary radial cracks in fragment 1 facing the clad crack at time t = 30 s (the colors show the associated crack strains).

There are at least three more possible reasons to the underestimation of fuel pellet swelling:

- fission-gas induced swelling might be underestimated at these high temperatures where very few experimental data are available (conversely, Fission Gas Release could be overestimated),
- the 2D(r,θ) configuration does not account for the potential axial fuel creep that might contribute to fill the space where the rigidity of the cladding is lost. In this respect, neutron radiography showed pronounced dish filling in most of the fuel pellets around the PPN in spite of the short holding time of 40 s at RTL. The limited axial extension of the clad cracks might therefore lead to a preferential fuel creep in the pellet parts facing opened clad cracks.
- water ingress might have led to fuel surface oxidation which is known to result in some non negligible expansion associated to grain-boundary cracking [10]. Extensive grain boundary separation is visible in the pellet region facing the clad crack, see the magnification of the CT1 cross-section in this region given in Figure 14. This is also the case in the CT2 cross-section where the clad defect is more important, see Figure 7.

While the first proposed explanation is difficult to investigate in more details due to the limited PIE available and to the non measurable FGR after the power ramp, the second one could be investigated by sophisticated 3D simulations that are out of the scope of the present work. With the model proposed by Lewis et al. [10] for CANDU fuels, the third explanation can however be assessed to some extent. This model describes high pressure steam oxidation of the fuel pellet surface in failed CANDU rods. According to Lewis et al. [10], the fuel surface oxidation kinetics is given by the following equation:

$$x_s(t) = x_e \left[1 - \exp\left(-\frac{S}{V}\sqrt{P_{H_2O}}\alpha t\right)\right] \quad (2)$$

where $x_s(t)$ is the fuel stoichiometry deviation at the pellet surface, x_e, the equilibrium stoichiometry deviation obtained by equating the oxygen potential in the fuel to that in the pellet-clad gap volume, S/V is the surface-to-volume ratio of the fuel (m), P_{H_2O} is the partial pressure of steam (in atm) in the gap volume and α is a surface exchange coefficient (m.s^{-1}). In practice, x_e, P_{H_2O} and α depend on temperature. Details on how these quantities are estimated are provided in Appendix A.

To analyze the potentiel increase of fuel stoichiometry during the HBC-4 power ramp, the 2D(r,θ) simulation results obtained 10 seconds after the formation of the through-wall crack (at t = 40 s) are here considered. The radial profile of temperature in the pellet fragment is given in Figure 16 (blue curve). The deformed pellet fragment facing the clad defect is also shown in Figure 16. As can be seen, the opening of the pellet crack facing the clad defect is limited by the compression stresses that hold at the hot pellet center. The pellet-clad gap is furthermore closed. The dashed line on the left marks the minimum radial position ($\sim$ 1.8 mm) where fuel crack oxidation by water is possible during the holding period at RTL (region where the pellet crack is opened). By using equation 2, the fuel stoichiometry deviation at the fuel crack surface can be calculated. Since a strong radial temperature gradient holds along the pellet radial crack, the fuel stoichiometry will vary significantly in the radial direction and increase towards the pellet center, as illustrated in Figure 16 (red curve). The fuel oxidation model shows that a fast oxidation of the fuel (in the 10 seconds at RTL that follow the formation of a through-wall crack)

is possible when the temperature exceeds 1700°C. A maximum stoichiometry deviation of 0.17 is reached at the radial position of 1.8 mm. In Figure 16, the dashed line on the right marks the maximum radial position (~ 3.4 mm) where a non negligible fuel stoichiometry deviation is calculated ($x_s > 0.01$). Closer to the pellet periphery, the temperature is too low to induce significant fuel oxidation ($x_s \sim 0$). The calculated fuel oxidized region (radius between 1.8 mm and 3.4 mm) is in very good agreement with the CT1 ceramography. Fuel swelling associated to grain boundary separation in consequence of fuel oxidation could therefore explain the underestimated fuel expansion.

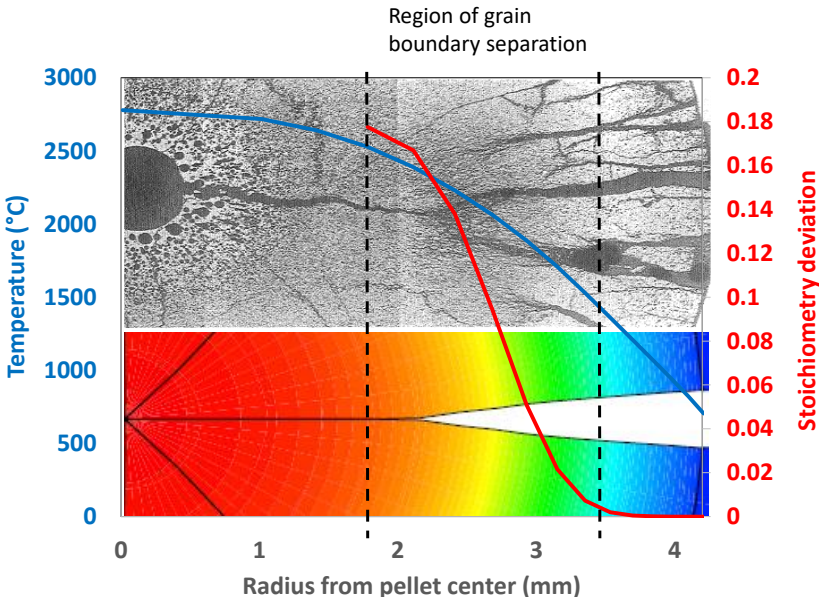

Figure 16: Calculated temperature and stoichiometry deviation profiles along the fuel pellet radial crack, 10 seconds after clad failure. The black dashed lines give the boundaries of the region where grain boundary separation is observed. The CT1 ceramography and the calculated pellet radial crack opening at the end of the holding time at RTL are superimposed.

Note that the calculations of the pellet radial crack opening has been the topic of extensive verification work in ALCYONE [21] and can be used in analyses with some confidence. Interestingly, the cold state of the pellet fragment facing the clad defect, calculated with the 2D(r,θ) scheme, bears some ressemblance with the CT1 ceramography, as shown in Figure 17. In particular, the 2D(r,θ) simulation indicates that a reopening of the main crack extending to the pellet center is likely at cold state with a partial closure at mid-radius.

Finally, it must be underlined that the CT2 ceramography presents some differences with CT1 that are obviously not catched by the 2D(r,θ) simulation. First, the excentricity of the central hole opposit to the clad crack. Second, the elliptic shape of the central hole. These differences may be related to a more advanced oxidation state of the fuel when compared to CT1. The greater crack opening could be at the origin of a more in-depth fuel oxidation that would lead to a more pronounced fuel swelling associated to grain boundary separation. This would apparently shift the

melted central region in the direction opposit to the clad crack. The elliptic shape of the central hole could be related to the water ingress closer to the pellet center with potential cooling of the fuel surface in front of the clad defect [13]. Overall, both phenomena (enhanced cooling by water ingress and steam oxidation) could have counterbalanced effects on the fuel central temperature leading to a melted fuel diameter of similar dimension than in the CT1 ceramography. This indicates that enhanced cracking of the cladding does not necessarily lead to additional melting of the fuel.

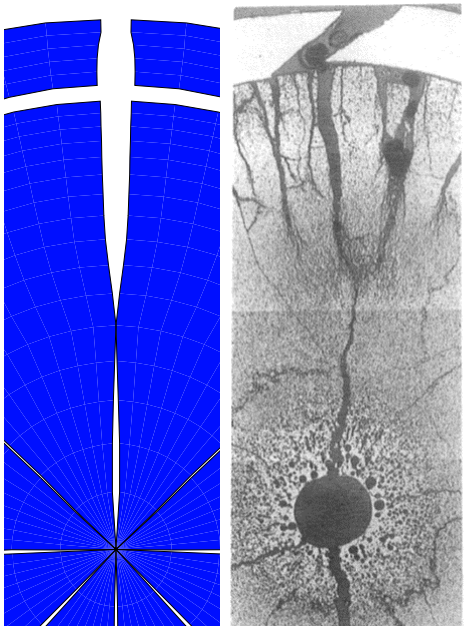

Figure 17: Calculated state of the fuel pellet main radial crack facing the clad defect after return at cold state, compared to the CT1 ceramography

VI. Conclusions

In this paper, advanced simulations of fuel melting and clad failure by I-SCC during a fast power ramp have been described, based on the 2D(r,θ) multi-fragment scheme available in the fuel performance code ALCYONE. The main purpose of this study was to investigate the impact of clad failure and water ingress on fuel temperature and melting. The following conclusions can be drawn:

- the thermodynamic based modeling of fuel melting integrated in ALCYONE led to a reasonable estimation of the melt diameter during the power ramp. The liquid fraction at the melted fuel boundary was found equal to 0.8;

- clad failure leads to a small increase of the fuel centerline temperature (40 °C) due to the increased clad and fuel diameters in consequence of the loss of the clad rigidity and of the water ingress that degrades the thermal conductivity of the gas mixture at the pellet-clad interface (assuming He is replaced by water vapor);

- the fuel temperature increase in consequence of the clad failure (40 °C) remains small when compared to that resulting from the experimental uncertainty on the LHGR (66.3 ± 4.6 kW.m^{-1} from gamma spectrometry measurements after the power ramp, 70.5 ± 7.1 kW.m^{-1} from online measurements of the thermal fluxes in the experimental loop). D'Ambrosi et al. [4] showed that the fuel temperature increase in a 1.5D simulation with +7 % LHGR (nominal 66 kW.m^{-1}) exceeded 100 °C.

- clad failure leads to a dissymetry in the fuel and clad diameters and to an excentricity of the melted fuel region in the direction of the clad crack;

- fuel pellet swelling during the power ramp cannot be attributed to thermal expansion and phase change only;

- enhanced fission gas induced swelling at temperatures close to fuel melting, preferential fuel creep at locations close to clad defects in consequence of the limited axial extension of the defects and grain boundary separation related to fuel oxidation by water vapor in the radial cracks facing the clad defect might all explain the underestimated swelling of the fuel in the 2D(r,θ) simulation.

To complete this work, the formation of the central hole related or not to fuel melting and fuel axial relocation could be included in the 2D(r,θ) simulation scheme, as proposed for instance by Novascone et al. [41] and Barani et al. [42]. The impact of the central hole on the fuel temperature and on the clad loading could then be investigated in more details. Fuel thermal conduction and melting dependent on fuel oxidation and intertitial oxygen diffusion could be added to better describe the consequences of water ingress in the rod. In this respect, a sophisticated coupled thermochemical - oxygen transport model based on the work of Welland [13] is already available in the PLEIADES computational environment [43] but needs to be adapted to the 2D(r,θ) geometry. Axial redistribution of fuel at the pellet center related to creep or melting could also be studied by 3D simulations of the HBC-4 power ramp.

References

[1] OECD/NEA FIDES, https://oecd-nea.org/jcms/pl_15313/framework-for-irradiation-experiments-fides.

[2] M. Bales, The Framework for IrraDiation experimentS (FIDES), in: TopFuel conference, Raleigh, North Carolina, USA, 2022.

[3] B. Boer, M. Verwerft, Qualification of the new Pressurized Water Capsule (PWC) for fuel testing at BR2, in: RRFM conference, Helsinki, Finland, 2021.

[4] V. D'Ambrosi, J. Sercombe, S. Béjaoui, al., P2M Simulation Exercise on past fuel melting irradiation experiments, submitted to Nuclear Technology, June 2022 (June 2022).

[5] V. D'Ambrosi, J. Sercombe, S. Béjaoui, al., P2M Simulation Exercise on past fuel melting irradiation experiments: main outcomes on fuel melting assessment in PWR fuel, in: TopFuel conference, Raleigh, North Carolina, USA, 2022.

[6] P. Blanpain, HBC Task 3 Power-to-Melt experiment, Tech. Rep. HBC 89/10, Belgonucléaire (1989).

[7] G. Bonny, P. Blanpain, D. Rozzia, S. Billiet, M. Verwerft, B. Boer, Re-evaluation of a power-to-melt experiment performed in the high burnup chemistry international program, submitted to Nuclear Technology, October 2022 (October 2022).

[8] B. Lewis, C. Phillips, M. Notley, A model for the release of radioactive krypton, xenon, and iodine from defective UO_2 fuel elements, Nuclear Technology 73 (1) (1986) 72–83.

[9] B. Lewis, Fundamental aspects of defective nuclear fuel behaviour and fission product release, Journal of Nuclear Materials 160 (2-3) (1988) 201–217.

[10] B. Lewis, B. Szpunar, F. Iglesias, Fuel oxidation and thermal conductivity model for operating defective fuel rods, Journal of Nuclear Materials 306 (1) (2002) 30–43.

[11] B. Lewis, W. Thompson, F. Akbari, D. Thompson, C. Thurgood, J. Higgs, Thermodynamic and kinetic modelling of fuel oxidation behaviour in operating defective fuel, Journal of Nuclear Materials 328 (2-3) (2004) 180–196.

[12] J. Higgs, B. Lewis, W. Thompson, Z. He, A conceptual model for the fuel oxidation of defective fuel, Journal of Nuclear Materials 366 (1-2) (2007) 99–128.

[13] M. Welland, B. Lewis, W. Thompson, Review of high temperature thermochemical properties and application in phase-field modelling of incipient melting in defective fuel, Journal of Nuclear Materials 412 (3) (2011) 342–349.

[14] B. Michel, C. Nonon, J. Sercombe, F. Michel, V. Marelle, Simulation of pellet-cladding interaction with the PLEIADES fuel performance software environment, Nuclear Technology 182 (2) (2013) 124–137.

[15] J. Sercombe, B. Michel, C. Riglet-Martial, O. Fandeur, 2.14 - Modelling of Pellet Cladding Interaction, in: R. Konings, R. Stoller (Eds.), Comprehensive Nuclear Materials, Elsevier, Oxford, 2020.

[16] B. Michel, I. Ramière, I. Viallard, C. Introini, M. Lainet, N. Chauvin, V. Marelle, A. Bouloré, T. Helfer, R. Masson, J. Sercombe, J. Dumas, L. Noirot, S. Bernaud, Two fuel performance codes of the PLEIADES platform: ALCYONE and GERMINAL, in: Nuclear Power Plant Design and Analysis Codes, Elsevier, 2021, pp. 207–233.

[17] C. Introïni, I. Ramière, J. Sercombe, B. Michel, P. Goldbronn, J. Fauque, PLEIADES/ALCYONE, a validated and predictive fuel performance code for modeling the behavior of PWR fuel rods, in: NUMAT conference, 2022.

[18] J. Sercombe, I. Aubrun, C. Nonon, Power ramped cladding stresses and strains in 3D simulations with burnup-dependent pellet–clad friction, Nuclear Engineering and Design 242 (2012) 164–181.

[19] B. Michel, J. Sercombe, G. Thouvenin, A new phenomenological criterion for pellet–cladding interaction rupture, Nuclear Engineering and Design 238 (7) (2008) 1612–1628.

[20] L. Noirot, MARGARET: A comprehensive code for the description of fission gas behavior, Nuclear Engineering and Design 241 (6) (2011) 2099–2118.

[21] J. Sercombe, R. Masson, T. Helfer, Stress concentration during pellet cladding interaction: Comparison of closed-form solutions with 2D(r,θ) finite element simulations, Nuclear Engineering and Design 260 (2013) 175–187.

[22] J. Sercombe, T. Helfer, E. Fédérici, D. Leboulch, T. Le Jolu, A. Hellouin de Ménibus, C. Bernaudat, 2D simulation of hydride blister cracking during a RIA transient with the fuel code ALCYONE, EPJ Nuclear Sciences & Technologies 2 (2016) 22.

[23] K. Lassmann, F. Hohlefeld, The revised URGAP model to describe the gap conductance between fuel and cladding, Nuclear Engineering and Design 103 (2) (1987) 215–221.

[24] P. Konarski, Thermo-chemical-mechanical modeling of nuclear fuel behavior. impact of oxygen transport in the fuel on Pellet Cladding Interaction, Ph.D. thesis, INSA Lyon, France (2019).

[25] OpenCalphad Software, http://www.opencalphad.com/.

[26] B. Sundman, U. Kattner, M. Palumbo, S. Fries, OpenCalphad - a free thermodynamic software, Integrating Materials and Manufacturing Innovation 4 (1) (2015) 1–15.

[27] C. Introïni, J. Sercombe, B. Sundman, Development of a robust, accurate and efficient coupling between PLEIADES/ALCYONE 2.1 fuel performance code and the Opencalphad thermochemical solver, Nuclear Engineering and Design 369 (2020) 110818.

[28] Thermodynamics Advanced Fuels-International Database, OECD/NEA Joint Project, 2013, https://www.oecd-nea.org/science/taf-id/.
[29] C. Guéneau, N. Dupin, L. Kjellqvist, E. Geiger, M. Kurata, S. Gossé, E. Corcoran, A. Quaini, R. Hania, A. Smith, et al., TAF-ID: An international thermodynamic database for nuclear fuels applications, Calphad 72 (2021) 102212.
[30] C. Guéneau, M. Baichi, D. Labroche, C. Chatillon, B. Sundman, Thermodynamic assessment of the uranium–oxygen system, Journal of Nuclear Materials 304 (2) (2002) 161–175.
[31] C. Guéneau, N. Dupin, B. Sundman, C. Martial, J.-C. Dumas, S. Gossé, S. Chatain, F. De Bruycker, D. Manara, R. Konings, Thermodynamic modelling of advanced oxide and carbide nuclear fuels: Description of the U-Pu-O-C systems, Journal of Nuclear Materials 419 (1-3) (2011) 145–167.
[32] M. Adamson, E. Aitken, R. Caputi, Experimental and thermodynamic evaluation of the melting behavior of irradiated oxide fuels, Journal of Nuclear Materials 130 (1985) 349–365.
[33] S. Yamanouchi, T. Tachibana, K. Tsukui, M. Oguma, Melting Temperature of Irradiated UO_2 and UO_2-2wt%Gd_2O_3 Fuel Pellets up to Burnup of about 30 GWd/tU, Journal of Nuclear Science and Technology 25 (6) (1988) 528–533.
[34] V. D'Ambrosi, J. Sercombe, S. Béjaoui, al., Presentation of the xM3 test case of the P2M simulation exercise and modeling with the fuel performance code ALCYONE, In preparation (September 2022).
[35] C. Mougel, B. Verhaeghe, C. Verdeau, S. Lansiart, S. Béguin, B. Julien, Power ramping in the OSIRIS reactor: database analysis for standard UO_2 fuel with Zy-4 cladding, in: Pellet-clad Interaction in Water Reactor Fuels, OECD NEA/6004, Aix-en-Provence, France, 2004.
[36] J. Sercombe, P. Konarski, C. Riglet-Martial, J. Julien, C. Introïni, D. Le Boulch, 3D modeling of PCI-SCC in ALCYONE fuel performance code, Tech. Rep. 1960, IAEA (2021).
[37] D. Le Boulch, M. Bono, E. Federici, N. Mozzani, L. Barbie, B. Baurens, V. Chabretou, Experimental characterization and modeling of I-SCC of zirconium alloy in an iodine vapor environment, Tech. Rep. 1960, IAEA (2021).
[38] P. Sens, The kinetics of pore movement in UO_2 fuel rods, Journal of Nuclear Materials 43 (3) (1972) 293–307.
[39] V. Arimescu, I. Vallejo, J. Karlsson, G. Zhou, G. Grandi, P. Raynaud, Y. Yun, N. Doncel, J. Sercombe, M. Pytel, R. Dunavant, J. Yoo, Third SCIP Modeling Workshop: Beneficial Impact of Slow Power Ramp on PCI Performance, in: Proceedings of WRFPM 2014, Sendai, Japan, Sep. 14-17, 2014, Paper No. 100045.
[40] B. Michel, J. Sercombe, G. Thouvenin, R. Chatelet, 3D fuel cracking modelling in pellet cladding mechanical interaction, Engineering Fracture Mechanics 75 (11) (2008) 3581–3598.
[41] S. Novascone, P. Medvedev, J. Peterson, Y. Zhang, J. Hales, Modeling porosity migration in LWR and fast reactor MOX fuel using the finite element method, Journal of Nuclear Materials 508 (2018) 226–236.
[42] T. Barani, I. Ramière, B. Michel, Analysis of fabrication and crack-induced porosity migration in mixed oxide fuels for sodium fast reactors by the finite element method, Journal of Nuclear Materials 558 (2022) 153341.
[43] C. Introïni, J. Sercombe, I. Ramière, R. Le Tellier, Phase-field modeling with the TAF-ID of incipient melting and oxygen transport in nuclear fuel during power transients, Journal of Nuclear Materials 556 (2021) 153173.
[44] B. Lewis, Prediction of the oxygen potential in the fuel-to-clad gap of defective fuel rods during severe accident conditions, Journal of nuclear materials 270 (1-2) (1999) 221–232.
[45] B. Lewis, B. Andre, B. Morel, P. Dehaudt, D. Maro, P. Purdy, D. Cox, F. Iglesias, M. Osborne, R. Lorenz, Modelling the release behaviour of cesium during severe fuel degradation, Journal of nuclear materials 227 (1-2) (1995) 83–109.
[46] P. Blackburn, Oxygen pressures over fast breeder reactor fuel (I:) a model for $uo_{2\pm x}$, Journal of Nuclear Materials 46 (3) (1973) 244–252.

Appendix A. Fuel surface oxidation model

Lewis et al. [10] proposed the following expression to describe the oxidation of the fuel pellet external surface in contact with the gap atmosphere, accounting for high pressure effects:

$$x_s(t) = x_e \left[1 - \exp\left(-\frac{S}{V}\sqrt{P_{H_2O}}\alpha t\right)\right] \tag{A.1}$$

where $x_s(t)$ is the fuel stoichiometry deviation at the pellet surface, x_e, the equilibrium stoichiometry deviation, S/V is the surface-to-volume ratio of the fuel (m^{-1}), P_{H_2O} is the partial pressure of steam in the gap and α is a surface exchange coefficient (m/s) given by:

$$\alpha = 0.365 \exp\left(-\frac{23500}{T}\right) \tag{A.2}$$

with the temperature T in K. A typical S/V ratio of 330 m^{-1} is proposed for CANDU fuels and has been considered also for the HBC-4 fuel. The calculation of the equilibrium stoichiometry deviation requires the estimation of the partial oxygen pressure P_{O_2} (atm) in the gap. This is done by solving the following cubic equation that results from mass balance considerations for the H and O in the gas mixture before and after steam dissociation [44][45]:

$$4(P_{O_2})^3 + 4[P^0_{H_2} - K^2_{H_2O}](P_{H_2})^2 + [(P^0_{O_2})^2 + 4P^0_{H_2O}K^2_{H_2O}]P_{O_2} - [(P^0_{H_2O})^2 K^2_{H_2O}] = 0 \tag{A.3}$$

with $P^0_{H_2O}$ and $P^0_{H_2}$ as the initial partial pressures of steam and hydrogen in the gap (atm). The equilibrium constant K_{H_2O} of the H_2O decomposition reaction ($H_2O = H_2 + \frac{1}{2}\,O_2$) is given by:

$$K_{H_2O} = \frac{P_{H_2}\sqrt{P_{O_2}}}{P_{H_2O}} = \exp\left(0.9794 \ln T - 1.1125 - \frac{28820}{T}\right) \tag{A.4}$$

The equilibrium stoichiometry deviation x_e is then obtained by solving the following equation based on the Blackburn thermochemical model [46]:

$$\ln P_{O_2} - 2 \ln \frac{x_e(2 + x_e)}{1 - x_e} - 108x_e^2 + \frac{32700}{T} - 9.92 = 0 \tag{A.5}$$

In the proposed application to the HBC-4 power ramp, the following partial pressures have been considered: $P^0_{H_2O} = 155$ atm, $P^0_{H_2} = 0$ atm.